Ti as Mediator in the Photoinduced Electron Transfer of Mixed-Metal NH_2-UiO66(Zr/Ti). Transient Absorption Spectroscopy Study and Application in Photovoltaic Cell.

Andrea Santiago Portillo,[a] Herme G. Baldoví,[b] Maria Teresa García Fernandez,[b] Sergio Navalón,[a] Pedro Atienzar,[b] Belen Ferrer,[a] Mercedes Alvaro,[a] Hermenegildo Garcia[b] and Zhaohui Li*[c]*

[a]Departamento de Química. Universitar Politécnica de Valencia. Camino de Vera s/n, 46022 Valencia.

[b]Instituto Universitario de Tecnologia Química, CSIC-UPV. Universitar Politécnica de Valencia, Av. de los Naranjos, 46022, Valencia.

[c]Research Institute of Photocatalysis, State Key Laboratory of Photocatalysis on Energy and Environment, Fuzhou University, Fuzhou, 350002, P. R. China.

AUTHOR INFORMATION

Corresponding Author

E-mail: hgarcia@qim.upv.es. Telephone: 96-3877000 ext. 78572

zhaohuili1969@yahoo.com.

ABSTRACT. A series of mixed-metal NH_2-UiO-66(Zr/Ti) with different percentages of exchanged Ti have been prepared and studied by transient absorption spectroscopy (TAS). The photo-generated transients from mixed NH_2-UiO-66(Zr/Ti) exhibit at short time scales two defined absorption bands, evolving to a continuous absorption band expanding from 300 nm to 700 nm at longer time scales. The observed spectral changes are compatible with an initial formation of Ti^{3+}-O-Zr^{4+} and its further transformation to Ti^{4+}-O-Zr^{3+} via metal-metal electron exchange, thus, providing support to the role of substituted Ti as mediator to facilitate electron transfer from excited ligand to the $(Zr/Ti)_6O_4(OH)_4$ nodes in mixed NH_2-UiO-66(Zr/Ti). The slow recombination of photo-generated electrons and holes in the mixed NH_2-UiO-66(Zr/Ti) has been advantageously used for the construction of a photovoltaic cell fabricated with the mixed NH_2-UiO-66(Zr/Ti), reaching higher photon-to-current efficiency than NH_2-UiO-66(Zr).

Introduction

The ever-increasing global demand for energy has stimulated a surge of research effort aimed at utilization of the solar energy [1-3]. One of the promising strategies is to directly transform solar energy to chemical energy by means of heterogeneous photocatalysis [4-10]. In addition to the commonly studied metal oxide semiconductors, metal-organic frameworks (MOFs), a class of 3D crystalline micro-mesoporous hybrid materials constructed from metal or metal clusters nodes interconnected by multi-dentated organic linkers, are emerging as a new type of promising photocatalysts due to their inherent large surface areas, uniform but tunable cavities and tailorable photoresponse [11-18]. Ever since the earlier work of Garcia et al. [19] and Majima et al. [20], which revealed the photo-induced electron transfer from the excited organic linker (terephthalate) to the metal–oxo cluster (Zn_4O_{13} quantum dot) on MOF-5, the applications of MOFs for photocatalysis, including hydrogen evolution [21-24], CO_2 reduction [25-28], organic transformations [29-35] and pollutant degradations [36-38], have attracted increasing attention [39]. What makes the MOFs especially appealing for photocatalysis is that light absorption in MOF materials can be relatively facilely tuned for better utilization of solar spectrum since the electronic properties of the MOF are usually determined by the interaction between the organic ligand and the metal ions. Due to the almost limitless combinations of metals and ligands, it is anticipated that a judiciously selection of the metal ions and organic linkers could led to optimized MOF structures for their use as photocatalysts. Actually, the advantageous tuning of the optical properties of the MOFs for photocatalysis has already been demonstrated via the replacement of metal ions, substitution of ligands or a combination of both [40-44].

Among all the MOF-based photocatalysts, NH_2-UiO-66(Zr), a robust Zr-containing MOF composed of hexameric Zr_6O_{32} units linked by 2-aminoterephthalic acid (ATA), is the one that has been probably most widely investigated [45-47]. A drawing of the NH_2-UiO-66(Zr) structure is shown in Fig S1. Although NH_2-UiO-66 has been used in a variety of photocatalytic applications, its performance is relatively low as compared with other already reported MOF-based photocatalysts, probably due to its inefficient charge transfer from the excited ligand (ATA) to the Zr-O clusters, which is believed to be the most general photochemical process in MOF-based materials [48]. Therefore, finding strategies to improve the efficiency of the charge

separation in NH_2-UiO-66(Zr) is relevant for its use in photocatalysis. Recently, Li et al. demonstrated that a partial substitution of Zr in NH_2-UiO-66(Zr) by Ti can improve the photocatalytic performance of this material for both H_2 evolution and CO_2 reduction [49]. Theoretical calculations reveal that the orbitals of Ti atoms make a significant contribution to the LUMO of this mixed-metal NH_2-UiO-66(Zr/Ti). Thus, quantum chemical modelling suggests that the presence of Ti results in a more favorable electron transfer from excited ATA to Zr-O clusters via the Ti atoms as mediators. Later on, Cohen et al. extended this strategy to the preparation of mixed-metal, mixed-ligand MOF based on NH_2-UiO-66(Zr) for enhanced CO_2 reduction by combining Zr-by-Ti exchange with the partial substitution of ligand to enhance the light absorption [50]. Although the promoting role of Ti on the photocatalytic performance of the mixed-metal NH_2-UiO-66(Zr) has been experimentally demonstrated, no transient absorption evidence supporting the proposed role of Ti as mediator has yet been provided for this system.

In this manuscript, a series of mixed-metal NH_2-UiO-66(Zr/Ti) with different percentages of exchanged Ti have been prepared and characterized by UV-visible absorption, emission spectroscopy and transient absorption spectroscopy (TAS). The results show that the photo-generated transient signals over mixed NH_2-UiO-66(Zr/Ti) evolved in the microsecond time scale, lending support to the role of Ti as relay facilitating the electron transfer from excited ATA to the $Zr_{6-x/}Ti_x$ nodes, where photocatalytic reduction should occur. This understanding has allowed us to fabricate a more efficient photovoltaic device based on mixed-metal NH_2-UiO-66(Zr/Ti).

Methods and Materials.

NH_2-UiO-66(Zr) was prepared following a previously reported procedure [49]. Substituted NH_2-UiO-66(Zr) with different percentages of Ti exchange, named NH_2-UiO-66(Zr/Ti), were prepared via post-synthetic exchange of the as-prepared NH_2-UiO-66(Zr) with $TiCl_4(THF)_2$ (THF: tetrahydrofuran) based on a previous report [49]. The percentage of substituted Ti was determined by Inductively Coupled Plasma Optical Emission Spectrometry (ICP-OES). Before ICP-OES experiment, the solid samples were digested in a mixture of HNO_3 and milli-Q water.

TAS measurements were performed employing the third harmonic (355 nm) of a Nd:YAG laser (25 mJxpulse, 7 ns fwhp). The photoluminescence (PL) quantum yields and lifetimes were measured employing acetonitrile suspensions of the MOFs matched to the same absorbance at the excitation wavelength (350 mn) with triphenylpyrylium used as standard to determine PL quantum yields.

The photovoltaic cell was fabricated on Indium titanium oxide (ITO)-coated glass substrate using the MOF as the photoactive layer and its configuration is shown in supporting Fig S2. The ITO was first cleaned by ultrasonic agitation in acetone and isopropanol and after drying, it was covered with a dense TiO_2 layer using spin coating. A layer of MOFs with a thickness of 1.5 μm was used as the photoactive component. The device is completed by a gold cathode previously coated with a thin layer of Spiro-MeOTAD as hole transport layer. The thickness of all of the films was measured by a MicroXAM-100 3D surface profilometer.

To determine the J_{SC}-V_{OC} plots, the cell was connected to a source Meter (Keithley 2601). The voltage scan was controlled using ReRa Tracer software. The data were automatically transferred to a PC that controlled the experiment and at the same time provided data storage capability to the system. The solar simulator (Sun 2000, ABET Technologies) was equipped with an AM 1.5G filter and the nominal power for the measurements was 100 mW/cm^2. The same cells were used to record the incident photon to current efficiency (IPCE) spectra. In IPCE measurements, the cell was illuminated with a 150 W xenon lamp through a Czerny-Turner monochromator. The current output at short circuit was measured by a potentiostat (AMEL), which transferred the data through the A/D converter card to the PC controlling the monochromator apparatus. IPCE curves were calculated using a Newport (818-UV-L) calibrated photodiode.

Results and Discussions

Mixed-metal NH_2-UiO-66(Zr/Ti) with different percentage of Ti were prepared by dispersing NH_2-UiO-66(Zr) in anhydrous N,N-dimethylformamide (DMF) containing different $TiCl_4(THF)_2$ concentration in the range of 17.1 to 34.3 g L^{-1} under inert atmosphere for 96 h. ICP measurements revealed that 17.6%, 25%, 28.5% and 35% of Zr in NH_2-UiO-66(Zr) have been

replaced by Ti (Table S1). All the exchanged samples show similar X-ray diffraction (XRD) patterns as that of pure NH_2-UiO-66(Zr), except that the 2θ value at around 7.31º observed for all NH_2-UiO-66(Zr/Ti) shifts to a higher value (Fig. 1A). Such shift is a consequence of the shrinking of the crystal lattice due to the substitution of larger Zr^{4+} by smaller Ti^{4+} ions, a phenomenon previously reported and frequently observed on inorganic semiconductor solid solutions [51]. The shrinking of the crystal lattice is also reflected in the lattice parameters which have been obtained from the analysis of the XRD patterns, considering that the MOFs crystallize in the cubic system, as it has been previously reported [45]. The lattice parameter for pure NH_2-UiO-66(Zr) and metal-substituted NH_2-UiO-66(Zr/Ti-35%) is 20.7950(13) Å and 20.7482 (9) Å, respectively. Miller indices for all peaks present in the XRD patterns of pure NH_2-UiO-66(Zr) and substituted NH_2-UiO-66(Zr/Ti) are shown in Fig. 1A and also in table S2. The absence of the amorphous Ti moiety was confirmed by the N_2 adsorption/desorption isotherms (Fig. S3). The series of Ti substituted NH_2-UiO-66(Zr/Ti) show a BET specific surface area in the range of 800-670 $m^2 g^{-1}$ (Fig. S3), which are comparable to that observed over pure NH_2-UiO-66(Zr) (890 $m^2 g^{-1}$). In addition to two main peaks at around 265 and 365 nm which can be attributable to the absorption of Zr–O clusters and ligand-based absorption in NH_2-UiO-66(Zr) respectively, the UV-visible diffuse reflectance spectra (DRS) of all the mixed-metal NH_2-UiO-66(Zr/Ti) show an extra shoulder peak extending to ca. 500 nm, a feature assigned to the interaction between the ligand and Ti^{4+} ions (Fig. 1B). The mixed-metal NH_2-UiO-66(Zr/Ti) with different percentage of Ti have been fully characterized by Attenuated total reflection-Fourier transform infrared (ATR-FTIR) spectroscopy, thermogravimetry and Scanning electron microscopy (SEM) (supporting Figure S4-S6). Although analyses by X-ray photoelectron spectrum (XPS) and X-ray absorption fine structure (XAFS) would be necessary to determine the structure of the prepared materials as well as to further rule out the possibility of the formation of Ti impurities, all the available characterization data suggest that the mixed NH_2-UiO-66(Zr/Ti) have been successfully obtained as it has been previously reported [49]. In this context, it is worth mentioning that in the previous article where the Ti subtituted NH_2-UiO-66(Zr/Ti) was synthesized for the first time, XPS and XAFS analyses were carried out [49]. The XPS showed two peaks in the Ti 2p region, corresponding to Ti 2p3/2 and Ti 2p1/2, providing confirmation of the successful incorporation of the Ti in the NH_2-UiO-66(Zr). The XFAS analyses supported the successful substitution of Zr by Ti. It is reported that the local environment of Ti in NH_2-UiO-66(Zr/Ti) was eight-fold

coordinated with two short and six long Ti-O bonds, similar to the coordination environment observed on the Zr in pure NH_2-UiO-66(Zr), indicating that Ti is surely substituted into the NH_2-UiO-66(Zr) framework.

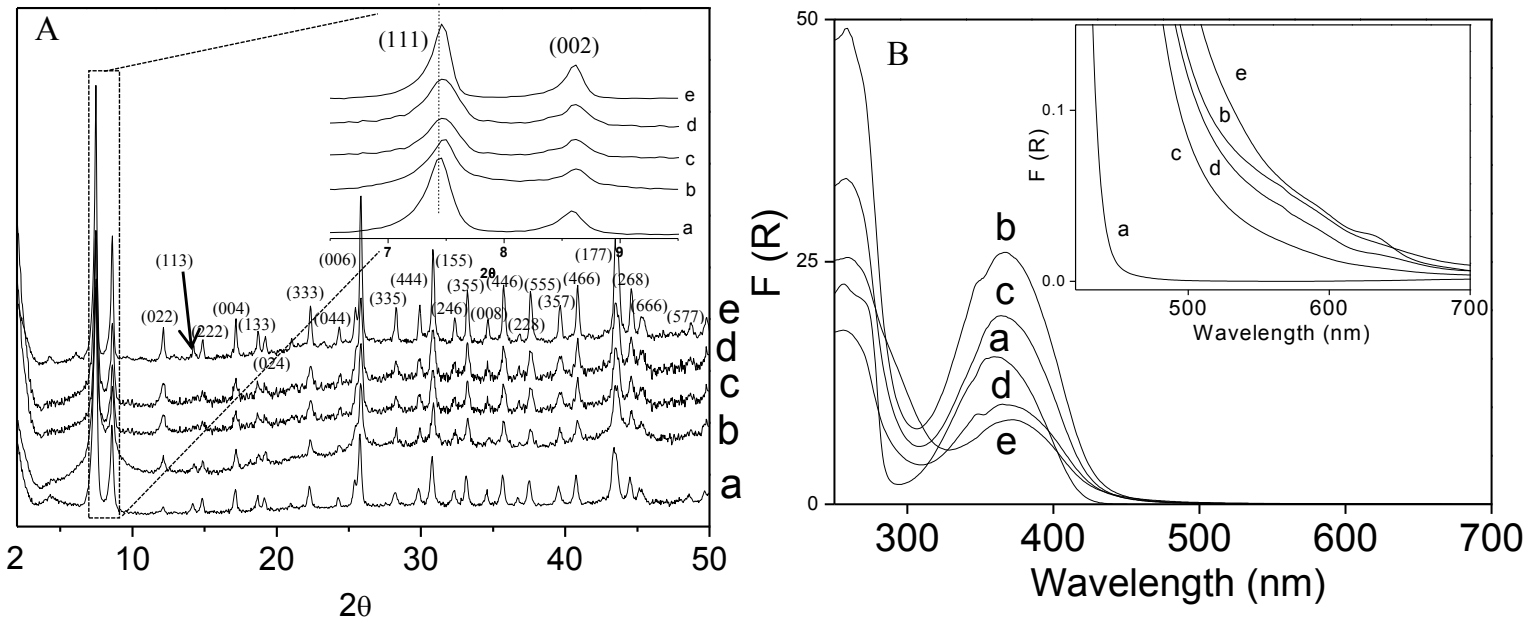

Figure 1 (A) XRD patterns of pure NH_2-UiO-66(Zr) (a) and mixed-metal NH_2-UiO-66(Zr/Ti) with %Ti 17.6 (b), 25 (c), 28.5 (d) and 35 (e). The inset shows the magnification of the 2θ region from 7 to 9°. (B) UV-vis DRS (plotted as the Kubelka-Munk function of the reflectance) of the mixed-metal NH_2-UiO-66(Zr/Ti) with %Ti: 0 (a), 17.6 (b), 25 (c), 28.5 (d) and 35 (e) (inset in B a magnification in the visible light region).

To gain better understanding on the process of photo-excited charge separation in the mixed-metal NH_2-UiO-66(Zr/Ti), TAS was carried on the mixed NH_2-UiO-66(Zr/Ti) and was compared with that of pure NH_2-UiO-66(Zr). Figure 2A shows the diffuse reflectance transient absorption spectra recorded at two different times after 355 nm laser pulse for pure NH_2-UiO-66(Zr) under N_2 atmosphere. These transient absorption spectra show the bleaching of the ground state at around 360 nm that extends even 25 μs after the laser pulse and an absorption band centered at 420 nm. Fig. 2B shows representative signal decays at different wavelengths. The lifetime of transient species responsible for the 420 nm peak was determined from the best

fit of the signal monitored at 420 nm to the sum of two mono-exponential kinetic with τ_1 = 11.4±1.0 μs (67%) and τ_2 = 98.9±23.7 μs (33%). The lifetime values are given with the standard error afforded by the fit. To determine the nature of the 420 nm transient species, quenching experiments were performed. The temporal profile of the signal monitored at 420 nm for NH_2-UiO-66(Zr) was partially quenched by oxygen, a typical triplet and electron quencher, and dichlorometane which is a well known electron quencher, while it grows in the presence of methanol, a well known hole quencher (Supporting Figure S7). This behavior indicates that the transient species absorbing at this wavelength generated on pure NH_2-UiO-66(Zr) should be a combination of triplet excited state and trapped electrons.

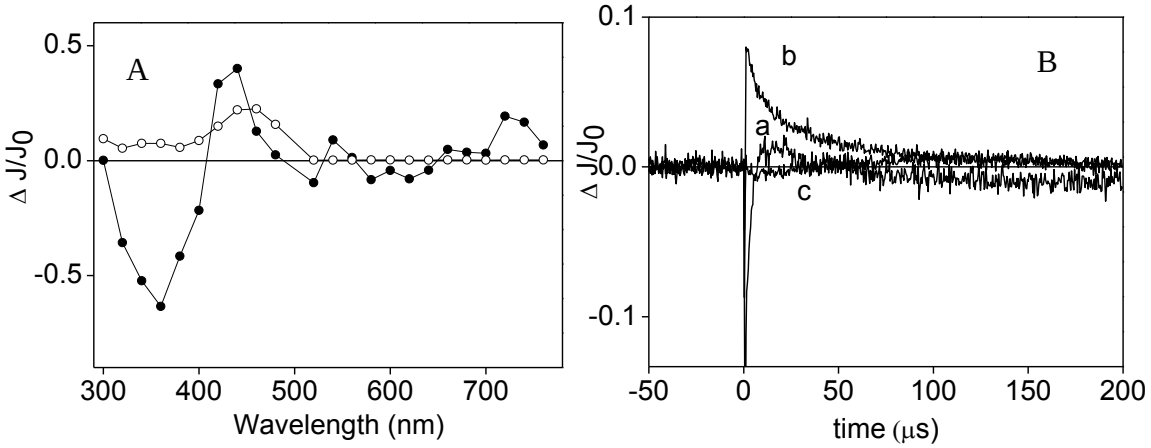

Figure 2 (A) Diffuse reflectance TA spectra recorded 2.8 (●) and 199 (❍) μs after 355 nm laser pulse under nitrogen atmosphere for NH_2-UiO-66(Zr); (B) Temporal profile of the signals monitored at 300 (a), 420 (b) and 550 (c) nm after 355 nm laser pulse under nitrogen atmosphere for NH_2-UiO-66(Zr).

To rationalize where these trapped electrons are located on the MOF, TAS measurements of an aqueous solution of 2-aminoterephthalic acid (ATA) at pH 10 have been performed. 355 nm laser excitation on the aqueous ATA solution allowed us to record a transient absorption spectrum exhibiting two maxima at 345 and 505 nm and a small band peaking at 720 nm in the far red end of our photomultiplier detector (Fig. 3). The two bands centered at 345 and 505 nm are completely quenched by oxygen, indicating that they correspond to triplet excited state (Supporting Figure S8). The lifetime of the ATA triplet excited state obtained from the best fit of

the temporal profile of the signal monitored at 505 nm to a sum of two monoexponential kinetics is τ_1 = 82.3±4.6 μs (64%) and τ_2 = 487.1±24.1 μs (36%). The lifetime values are given with the standard error afforded by the fit. It is interesting to note that the temporal profile of the signal monitored at 345 nm does not decay completely even 4000 μs after the laser pulse. However, this long-lived component disappears when the sample was diluted (Supporting Figure S9). This behavior indicates that an intermolecular photo-induced electron transfer process between two 2-aminoterephthalate molecules could occur after excitation. The small absorption band centered at 720 nm is characteristic of solvated electrons in water and indicates that photo-induced electron ejection from excited ATA to H_2O also occurs. Such electron photo-ejection has previously been reported for sodium terephthalate [58]. The addition of Zr^{4+} to an aqueous solution of 2-aminoterephthalate caused the quenching of both the maximum initial intensity and the lifetime of the signals assigned to the ATA triplet excited state (inset of Fig. 3). The rate constant k_q for the dynamic triplet quenching by Zr^{4+} was determined to be $4.0x10^7 \pm 1.4x10^7$ $M^{-1}s^{-1}$. This k_q has also been determined employing ethanol as solvent ($5x10^7 \pm 1x10^7$ M^{-1}s-1) for a posterior comparison with Ti^{4+} quenching (vide infra). The quenching rate constants k_q values are given with the absolute error. The addition of Zr^{4+} also quenched the signal at 720 nm, indicating that solvated electrons are generated in lesser amounts as a consequence of electrons trapped by Zr^{4+}. The transient spectrum in the presence of Zr^{4+} could be attributed to the formation of a geminated pair of Zr^{3+} and 2-aminoterephthalate radical monoanion. Taking into account the electron donor capability of 2-aminoterephthalate dianion upon photo-excitation in water, quenching of ATA excited state by Zr^{4+} can be considered as an electron transfer. In any case, the quenching experiments of ATA excited state in water by Zr^{4+} conclusively shows the occurrence of static and dynamic interactions during the lifetime of ATA excited states and Zr^{4+}.

Based on the TAS measurements in aqueous solution, the transient species observed upon excitation of pure NH_2-UiO-66(Zr) can be reasonably attributed to photo-excited electrons most probably trapped by Zr^{4+} in the Zr_6O_{32} clusters, with the positive holes located on the ATA ligand being not detectable in the transient spectrum. The absorption spectrum of the photo-excited electrons on the NH_2-UiO-66(Zr) differs from that of the geminated pair of Zr^{3+} and 2-aminoterephthalate radical monoanion in solution due to the existence in the MOF of well-defined Zr_6O_{32} clusters that are probably not present in aqueous solution. On the other hand, due to the nature of the quenching experiment with an excess of ATA, the transient spectrum in

aqueous solution is dominated by absorption of ATA species that are, however, not prevalent in the transient spectrum of solid NH_2-UiO-66(Zr) that corresponds mainly to electrons. Although it has been recently reported that a direct electron transfer from the excited ATA to Zr^{4+} in NH_2-UiO-66(Zr) is kinetically unfavorable [48], our previous studies revealed that the photo-induced electron transfer from the excited ATA to Zr oxo-clusters in NH_2-UiO-66(Zr) does occur with sufficient efficiency to be spectroscopically detectable, based on the photoluminescence studies, as it was also confirmed by ESR analysis [27]. Here, the experimental TAS also provided evidence to support that electron transfer from the excited ligand (ATA) to Zr_6O_{32} clusters to form Zr^{3+} occurs in pure NH_2-UiO-66(Zr) when irradiated.

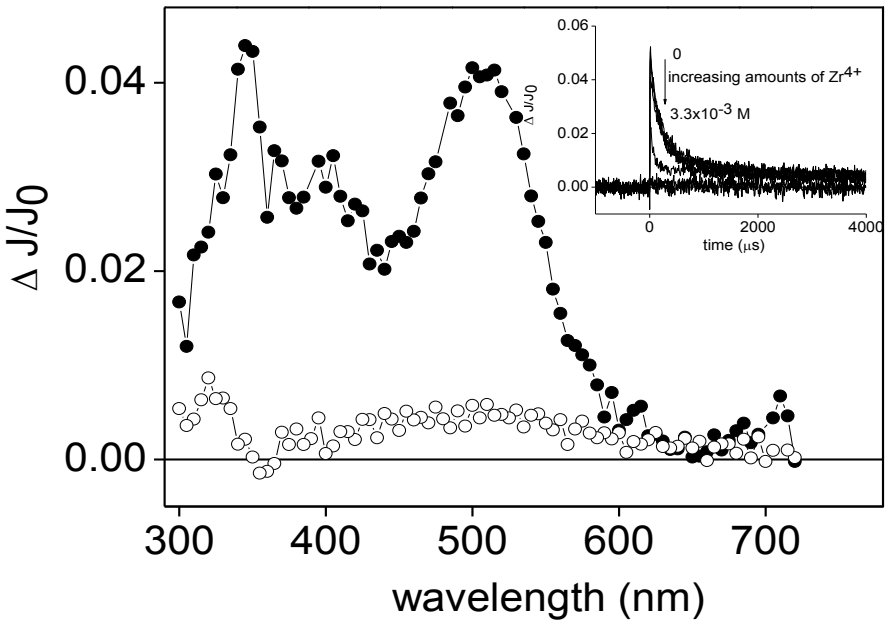

Figure 3 Transmission UV-visible TA spectra recorded 52 μs after 355 nm laser pulse under inert atmosphere for an aqueous solution of 2-aminoterephthalic (ATA) (pH 10, $2.9x10^{-4}$ M, before (●) and after (❍) the addition of an aqueous solution of Zr^{4+} ($3.3x10^{-3}$ M). The inset shows the temporal profile of the signals monitored at 345 nm after 355 nm laser pulse under inert atmosphere of an aqueous solution of (ATA) (pH 10, $2.9x10^{-4}$ M upon addition of increasing amounts of Zr^{4+} from 0 to 3.3 mM.

In contrast, the TA spectra recorded for mixed NH_2-UiO-66(Zr/Ti) are different from that of single metal NH_2-UiO-66(Zr), a fact that is in agreement with the experimentally observed influence of Ti-exchange in the photocatalytic reactions. The diffuse reflectance TA spectra recorded at short times (< 3 μs) after the 355 nm laser pulse for NH_2-UiO-66(Zr/Ti-35%) shows the appearance after the laser pulse of two defined absorption bands, one of them a more intense absorption band centered at 450 nm and the second one a less intense, but broader band peaking at 540 nm (Fig. 4a).

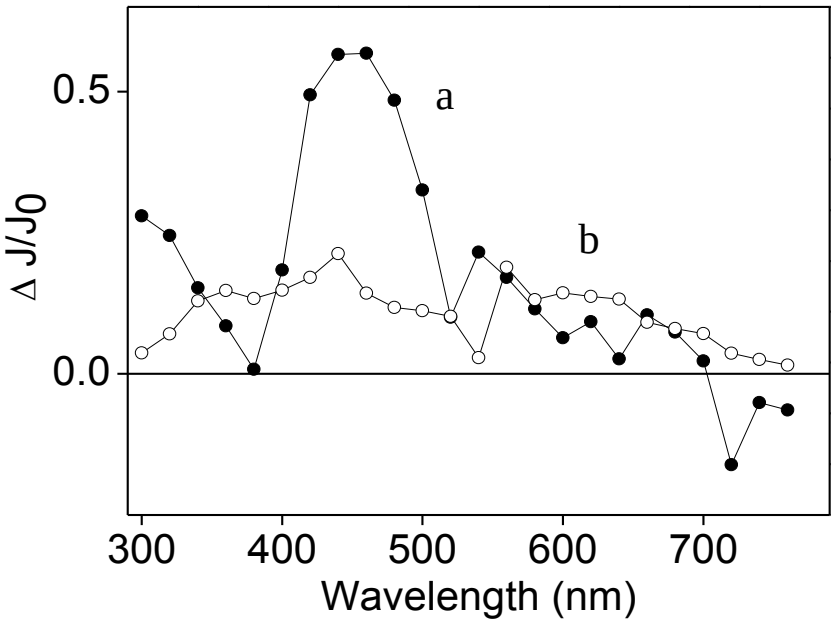

Figure 4 UV-vis DRS TA spectra recorded (a) 3 (●) and (b) 184 (❍) μs after 355 nm laser pulse under nitrogen atmosphere for NH_2-UiO-66(Zr/Ti-35%).

The temporal profile of the signals monitored at 450 nm and 540 nm for NH_2-UiO-66(Zr/Ti-35%) are different in the time window up to 200 μs, indicating that they should correspond to at least two different transient species (Fig. 5A). The lifetime of this transient species was determined from the best fit of the temporal profile monitored at 450 nm to the sum of two mono-exponential kinetic with τ_1 = 8.6 ± 2.3μs (45%) and τ_2 > 200 μs (55%) and from the best fit of the temporal profile monitored at 540 nm to a monoexponential growth τ_1'(growth) = 8.5 ± 2.5 μs. The lifetime values are given with the standard error afforded by the fit. It is interesting to note that the short lifetime component of the decay of the transient signal absorbing at 450 nm coincides with the growth lifetime of the transient species absorbing at 540 nm. This

indicates that the formation of the transient species absorbing at 540 nm comes in a percentage about 40 % from the disappearance of the short-lived transient species absorbing at 450 nm. Quenching experiments for the mixed-metal NH_2-UiO-66(Zr/Ti-35%) show that the signal at 540 nm is quenched by dichlorometane and grows in the presence of methanol, indicating that it corresponds to trapped electrons, but located in a different environment than in pure NH_2-UiO-66(Zr) (Supporting Figure S10). However, unlike that in pure NH_2-UiO-66(Zr), the transient signal at 450 nm is weakly affected by the quenchers, which may imply an overlapping of transient species, probably located on the ATA ligand, absorbing at this wavelength (Supporting Figure S11).

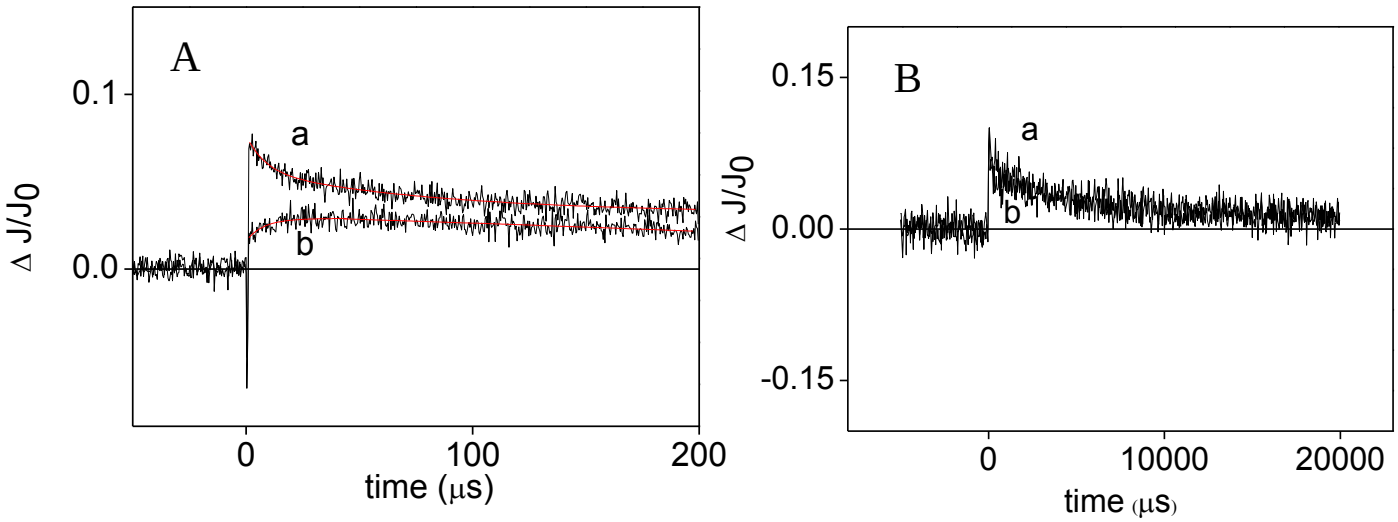

Figure 5. Temporal profile of the signals monitored at (a) 450 and (b) 540 nm after 355 nm laser pulse under nitrogen atmosphere for NH_2-UiO-66(Zr/Ti-35%) in two different time windows: (A) 200 μs and (B) 20 ms. The red line corresponds to the best fit of the signal to a sum of two monoexponential kinetics for 450 nm: τ_1 = 8.6±2.3 μs (45%) τ_2 > 200 μs (55%) and to a monoexponential growth for 540 nm: τ_1' (growth) = 8.5±2.5 μs. The lifetime values are given with the standard error afforded by the fit.

Again, to rationalize where these trapped electrons are located on the NH_2-UiO-66(Zr/Ti), TAS measurements of the ATA ligand in solution in the presence of Ti^{4+} have been performed. In this liquid phase quenching experiments, ethanol has been employed as solvent due to the instability

of the Ti^{4+} cation in water. Similarly to the TA spectrum in H_2O shown in Figure 3, the transient absorption spectra of an ethanol solution of the ATA ligand upon 355 nm laser excitation show two maxima at 320 and 505 nm (Supporting Figure S12). The two bands centered at 320 and 505 nm were quenched by oxygen, indicating that they correspond to triplet species. The lifetime of the ATA triplet excited state obtained from the best fit of the temporal profile of the signal monitored at 505 nm to a monoexponential kinetics is $\tau = 52.8 \pm 0.7$ μs. The lifetime value is given with the standard error afforded by the fit. Addition of Ti^{4+} to an ethanol solution of ATA caused the quenching of both the maximum initial intensity and the lifetime of the signals attributed to the ATA triplet excited state (Supporting Figure S11). The rate constant k_q for the dynamic triplet quenching by Ti^{4+} was determined to be $4.1 \times 10^8 \pm 4.5 \times 10^7$ $M^{-1}s^{-1}$. The quenching rate constant k_q value is given with the absolute error. The dynamic quenching of the ATA triplet by Ti^{4+} can be considered as an electron transfer from the ATA excited state to Ti^{4+} and occurs about one order of magnitude faster for Ti^{4+} than for Zr^{4+}, based on the comparison of the corresponding quenching rate constants.

Based on the results of TAS measurements in solution, the transient signal monitored at 540 nm recorded upon NH_2-UiO-66(Zr/Ti) excitation can be assigned to Ti^{3+}. The formation of Ti^{3+} species by a ligand to metal charge transfer process upon excitation of MIL-125(Ti)-type MOFs and other related materials have been previously demonstrated clearly by EPR spectroscopy, flash photolysis and theoretical studies [23, 52-57]. This assignment is in agreement with the wavelength maximum reported for electrons trapped in Ti^{4+} in other cases.[52-57] The short-lived component of the transient signal absorbing at 450 nm recorded upon NH_2-UiO-66(Zr/Ti) excitation could be attributed to the triplet excited state of the ATA ligand in the MOF. Taking into account that the formation of the Ti^{3+} species comes, at least in 40 %, from the disappearance of the excited state of the ATA ligand, it is evident that a ligand-to-metal electron transfer process takes place in the microsecond time scale from triplet excited ATA to Ti^{4+} of the Ti/Zr-O cluster to form the Ti^{3+} species (Scheme 1). The TAS data indicate that Ti^{3+}, more exactly should be Ti^{3+}-O-Zr^{4+} in a $(Ti/Zr)_6O_4(OH)_4$ node, should be formed in two different mechanisms. One of them instantaneous in the time scale of our ns laser system and a second one in 40 % proportion through the intermediacy of ATA triplet excited state. Then, the long-lived component of the transient signal absorbing at 450 nm should be attributed to the remaining positive hole located on the ATA ligand. Two possible localizations of the positive charge carrier

on the ATA ligand are proposed and shown in Scheme 1, based on the different electronic structure of the functional groups present in the ATA ligand. In one of them, the radical cation is located on the N atom of the amino group and in the other one, the positive charge is located on one of the oxygen atoms of the carboxylate group. Taking into account that the original ATA ligand bears two negative charges, located on the oxygen atoms of the two carboxylate groups, the total charge on the ATA ligand upon transferring one electron to the inorganic cluster is a radical anion. It is interesting to mention that the fact that the radical cation centered on the N atom of the amino group of the ATA ligand is immobilized on the crystalline framework of the MOF rules out the possibility of further chemical transformations such as polycondensations, typical for free amines.

Different to the case of pure NH_2-UiO-66(Zr), the TA spectra recorded for mixed-metal NH_2-UiO-66(Zr/Ti) change significantly at long delay times. Thus, longer than 200 μs after the laser pulse, the TA spectrum of the mixed-metal NH_2-UiO-66(Zr/Ti-35%) consists of a continuous absorption band expanding from 300 nm to 700 nm (Fig. 4b). After different initial decays, at time scale beyond 20 μs, the temporal profile of the signal monitored at any wavelength from 300 to 700 nm are coincident, indicating that at this time delay they probably correspond to the same transient species (Fig. 5B). Such a phenomenon indicates that the initially formed localized Ti^{3+}-O-Zr^{4+} has changed to another transient species, which is assumed to be the delocalized, non/geminate photo-induced charge separated state with electrons trapped in the inorganic clusters, as Ti^{4+}-O-Zr^{3+}, and positive holes on the ATA ligand based on previous TAS studies [19,58]. The transformation from Ti^{3+}-O-Zr^{4+} present at short time scales to Ti^{4+}-O-Zr^{3+}at longer time scales is consistent with previous theoretical calculations predicting that Ti acts as a mediator to promote the charge transfer from ATA ligand to Zr center in mixed NH_2-UiO-66(Zr/Ti), a mechanism which was previously proposed based on the theoretical calculations (Scheme 1)

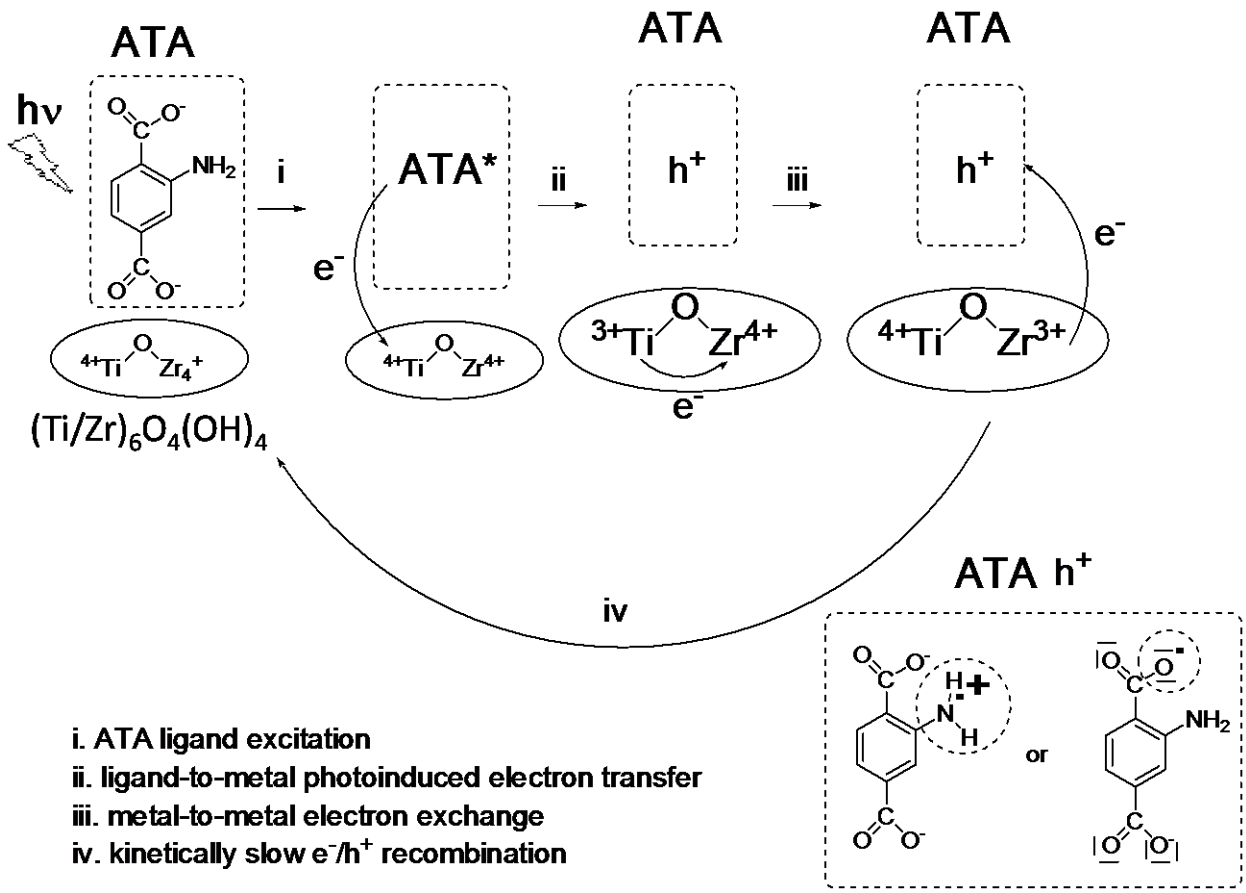

Scheme 1 Mechanistic proposal to rationalize the photochemical behavior of mixed NH_2-UiO-66(Zr/Ti).

Actually, although the previous discussion has been focused on NH_2-UiO-66(Zr/Ti-35%), the transient absorption spectra for all the MOFs of the series NH_2-UiO-66(Zr/Ti) are similar (Supporting Figure S13) and show analogous quenching behavior and spectroscopic properties at long times after the laser pulse (Supporting Figures S14-S15). Therefore, TAS provide evidence supporting that the photochemical behavior of mixed-metal NH_2-UiO-66(Zr/Ti), where Ti partially substitutes Zr, is different to that of single metal NH_2-UiO-66(Zr) and Ti^{4+} is the ion that initially accepts photo-generated electron from the excited ATA ligand to form Ti^{3+} in a $(Ti/Zr)_6O_4(OH)_4$ node. This process is easier for Ti^{4+} than for Zr^{4+}. The fact that the quenching rate constant of the ATA triplet by Ti^{4+} in solution is one order of magnitude higher than that determined for the quenching by Zr^{4+} also supports this rationalization. Subsequently, a metal-to-metal electron exchange would occur and the as-formed Ti^{3+}-O-Zr^{4+} is further transformed to Ti^{4+}-O-Zr^{3+}, which is presumably more active for the photocatalysis due to its much longer

lifetime. Therefore, with Ti acting as a mediator, the original inefficient pathway to form Zr^{3+} in pure NH_2-UiO-66(Zr) due to kinetically unfavorable direct electron transfer from the excited ATA to Zr^{4+} can take place in the mixed-metal NH_2-UiO-66(Zr/Ti) through Ti as mediator. Our TAS results provide direct evidence for the prompt and delayed formation of Ti^{3+} and subsequent Ti-to-Zr electron transfer at much longer time scales in the mixed NH_2-UiO-66(Zr/Ti). Although a similar metal-metal electron exchange process has already been reported in some bimetallic assemblies [59-61], the spectroscopic data obtained by TAS provide spectroscopic support to such a metal-metal electron exchange.

As a consequence of the introduction of Ti mediator, the transient state in the mixed NH_2-UiO-66(Zr/Ti), where electrons are delocalized on Zr/Ti clusters, should be longer lived due to the difficult charge recombination when delocalization takes place. In agreement with the kinetically slow Zr-ATA electron transfer, the lifetime of the photo-generated transient species for pure NH_2-UiO-66(Zr) is only 98.9±23.7 μs, while that for mixed NH_2-UiO-66(Zr/Ti-35%) is 19.9±6.1 ms, about three orders of magnitude longer live. The lifetime values are given with the standard error afforded by the fit. The significant increase of the lifetime of the transient species has also been observed for other mixed NH_2-UiO-66(Zr/Ti) at different Ti exchange levels (Supporting Table S3). The influence of the Ti content on the lifetime of the photo-induced charge separated state is again compatible with the role of Ti^{4+} in the $(Ti^{4+}/Zr^{4+})_6O_4(OH)_4$ clusters accepting the photo-generated electron from the excited ATA ligand.

The initial formation of Ti^{3+}-O-Zr^{4+} and its transformation to Ti^{4+}-O-Zr^{3+} upon excitation of mixed-metal NH_2-UiO-66(Zr/Ti) can also be evidenced by the photoluminescence (PL) spectroscopic studies. Similar to that of pure NH_2-UiO-66(Zr), when excited at 350 nm, the PL of the mixed NH_2-UiO-66(Zr/Ti) also shows a band centered at ca. 470 nm with a shoulder at around 530 nm (Fig. 6). However, these two bands are 10 nm red shifted as compared with those in pure NH_2-UiO-66(Zr). At the excitation wavelength, the ATA ligand is excited in both NH_2-UiO-66(Zr) and NH_2-UiO-66(Zr/Ti), and the PL emission should be originated from the radiative electron/hole recombination of geminate, localized charge separated states, ie, Zr^{3+} for NH_2-UiO-66(Zr) and Ti^{3+} for mixed-metal NH_2-UiO-66(Zr/Ti), to the ground state (S_0). The red-shift of the PL bands observed over mixed-metal NH_2-UiO-66(Zr/Ti) suggests that the recombination involves Ti^{3+} rather than Zr^{3+} when Ti is introduced into NH_2-UiO-66(Zr). The

first thing to note is that the electron transfer from Ti^{3+} in Ti^{3+}-O-Zr^{4+} to form Ti^{4+}-O-Zr^{3+} may well explain the decrease on the PL intensity of pure metal NH_2-UiO-66(Zr) when Ti is introduced into NH_2-UiO-66(Zr) and the ten times lower PL relative quantum yield for all mixed NH_2-UiO-66(Zr/Ti) as compared to NH_2-UiO-66(Zr) (Supporting Table S2). In addition, the PL lifetime for pure NH_2-UiO-66(Zr) is only 3.6±0.9 ns, while the introduction of Ti atoms into NH_2-UiO-66(Zr) leads to increased lifetime of the PL emission for all mixed NH_2-UiO-66(Zr/Ti), with the longest average lifetime of PL (24.5±1.7 ns) observed on NH_2-UiO-66(Zr/Ti-25%) (Supporting Table S4). The lifetime values are given with the standard error afforded by the fit. Such an increase in the PL lifetime suggests the existence of deeper trapped states for electron in the mixed-metal NH_2-UiO-66(Zr/Ti-25%), i.e. Ti^{3+} ions. The de-trapping of electrons from deeper trapped state (Ti^{3+}) gives the opportunity for a metal-metal electron exchange to occur efficiently.

To demonstrate the advantage of the Ti substitution in the photo-response of NH_2-UiO-66(Zr) and the occurrence of charge separation, the series of mixed-metal MOFs were used as the photoactive component in the fabrication of photovoltaic cells and their performance correlated as a function of Ti to Zr exchange. A pictorial representation of the operation of the device is shown in Scheme 2. A layer of MOFs with 1.5 μm was used as the photoactive part to generate the corresponding electron/hole pair upon illumination with a solar simulator. The positive holes generated in MOFs migrate to the gold electrode through the hole-transport layer, while the electrons migrate to the ITO electrode through the TiO_2 layer acting as electron transport layer. Figure 7 show the corresponding current density-voltage (J/V) curves measured for the photovoltaic cells constructed employing the pure NH_2-UiO-66(Zr) and two mixed-metal NH_2-UiO-66(Zr/Ti) as the photoactive component. The corresponding J/V curves under dark conditions have been also measured and shown in figure 7 to clearly distinguish the low current densities obtained for the devices under illumination from dark currents. As it can be seen in figure 7, the current densities measured under dark conditions are lower than 0.25 $\mu A/cm^2$, and therefore, it is expected small influence in the final current extracted under illumination. Table 1 summarizes the current densities, Jsc, voltages at open circuit, Voc, field factor, FF, and power conversion efficiency values obtained from the J/V curves under illumination shown in Figure 7. As shown in Table 1, under otherwise similar condition, the device fabricated from mixed NH_2-UiO-66(Zr/Ti-35%) showed higher J_{SC} as compared with those in pure NH_2-UiO-66(Zr),

indicating that NH_2-UiO-66(Zr/Ti-35%) exhibits a higher efficiency (one order of magnitude more efficient than NH_2-UiO-66(Zr)) in charge separation and mobility, leading to a more efficient conversion of light into current. The efficiency of the constructed optoelectronic devices is still low (incident photon to current efficiency of 0.1%), but serves to test the application of these MOFs as semiconductors and the role of Ti^{4+} promoting charge separation.

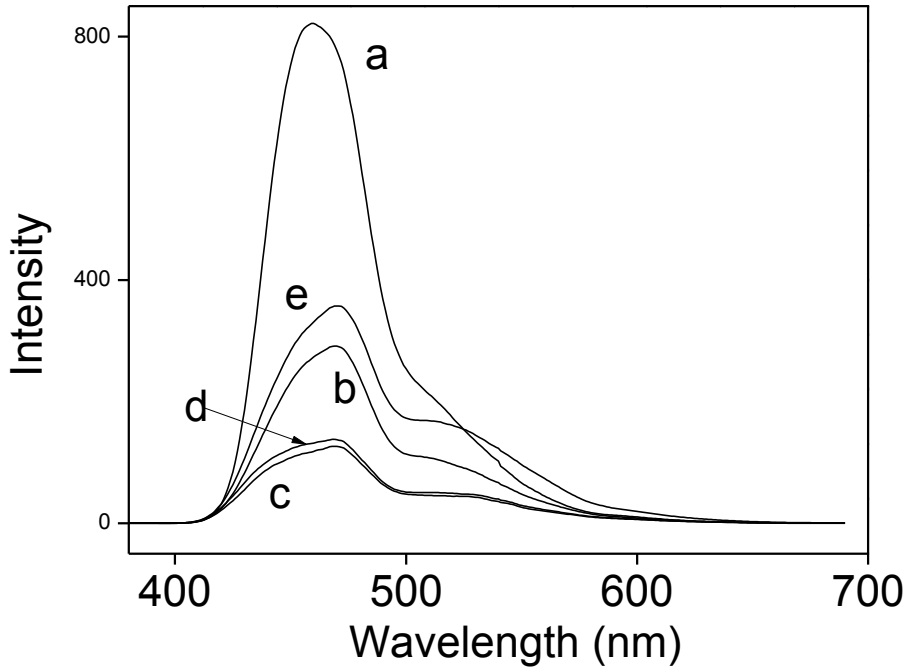

Figure 6 Photoluminescence spectra of the mixed-metal NH_2-UiO-66(Zr/Ti) with %Ti: 0 (a), 17.6 (b), 25 (c), 28.5 (d) and 35 (e) (λ_{ex} = 350 nm) recorded under nitrogen atmosphere.

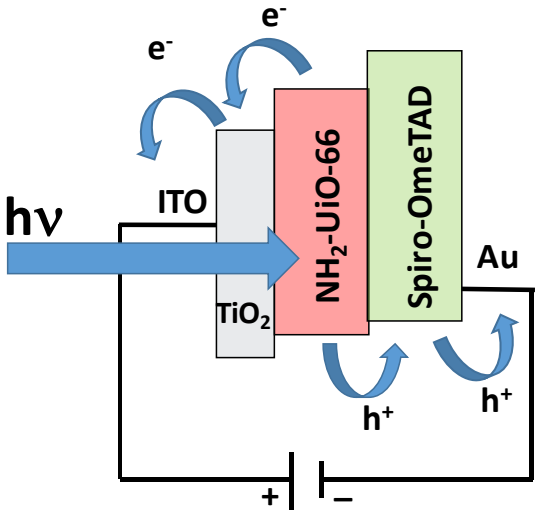

Scheme 2 A pictorial representation of the operation of the photovoltaic cells.

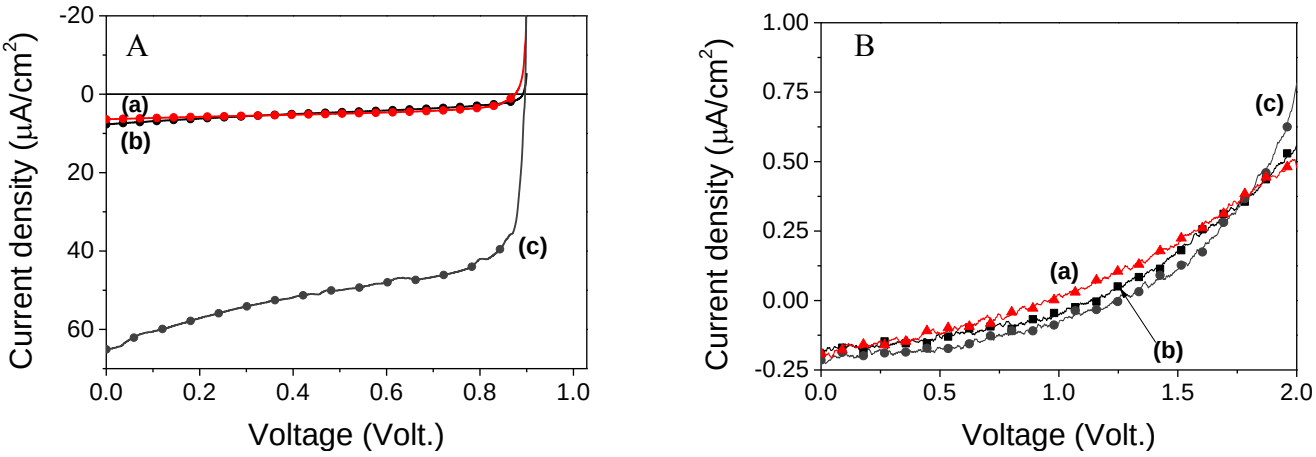

Figure 7. A) Current density–voltage characteristics measured under simulated AM1.5 solar irradiation (100 mW/cm^2, 1 sun) and B) Dark current density − voltage characteristics, for the photovoltaic cells constructed employing (a) NH_2-UiO-66(Zr), (b) NH_2-UiO-66(Zr/Ti-17.6%) and (c) NH_2-UiO-66(Zr/Ti-17.6%) as photoactive component.

MOFs	Jsc(μA/cm^2)*	Voc(mV)*	FF (%)*	Efficiency (%)*
NH_2-UiO-66(Zr)	6.39 ± 0.1	875.16 ± 5	53.16 ± 5	0.003 ± 0.001
NH_2-UiO-66(Zr/Ti-35%)	65.35 ± 0.1	885.62 ± 5	59.52 ± 5	0.034 ± 0.001
NH_2-UiO-66(Zr/Ti-17.6%)	7.69 ± 0.1	891.91 ± 5	37.05 ± 5	0.003 ± 0.001

*Measured under solar simulator (ABET Technologies) equipped with an AM 1.5G filter and the nominal power for the measurements was 100 mW/cm^2 and the temperature 25°C.

Table 1. Performance parameters of three photovoltaic devices based on NH_2-UiO-66 as photoactive material. The Jsc, Voc, FF and efficiency values are given with the standard error.

We have been able to measure the photocurrent spectra of these optoelectronic devices. Figure 8 shows that employing NH_2-UiO-66(Zr/Ti-35%) as active layer, the device is able to

generate current at longer wavelengths than employing pure NH_2-UiO-66(Zr) reaching the visible region of the spectra. This result supports the previous conclusion that the Ti-substituted MOFs improve the performance of the devices by enhancing the visible light photo/response.

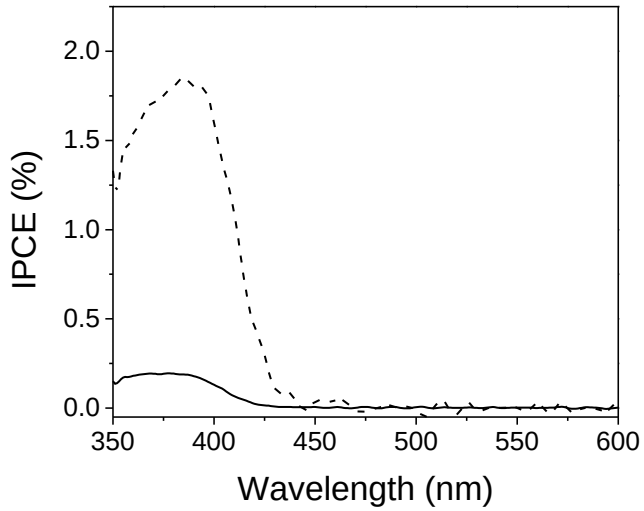

Figure 8. Photocurrent spectra of the photovoltaic devices employing pure NH_2-UiO-66(Zr) (solid) and mixed-metal NH_2-UiO-66(Zr/Ti-35%) (dashed) as active layer.

Conclusions

In summary, the TA spectra recorded for mixed-metal NH_2-UiO-66(Zr/Ti) upon irradiation evolve from a spectrum at short delay times exhibiting two absorption bands to a continuous absorption band ranging from 300 nm to 700 nm at longer time scale, the evolution being compatible with an initial formation of Ti^{3+} and its further transformation to Zr^{3+} when mixed-metal NH_2-UiO-66(Zr/Ti) is excited. This change in the transient spectrum does not occur for single metal NH_2-UiO-66(Zr) for which only a transient spectrum consisting in bleaching of the NH_2-UiO-66(Zr) ground state absorption and a peak at 420 nm is recorded. The present study provides spectroscopic evidence supporting the role of substituted Ti as a mediator to facilitate the electron transfer from excited ATA ligand to the Zr nodes in mixed NH_2-UiO-66(Zr/Ti). The existence of a trapping electron state (Ti^{3+}) in the mixed NH_2-UiO-66(Zr/Ti) allows more efficient metal-metal electron exchange and should account for the enhanced photocatalytic performance observed for mixed NH_2-UiO-66(Zr/Ti). Taking advantage of the slow recombination between the photo-generated electrons and holes in the mixed NH_2-UiO-

66(Zr/Ti), a photovoltaic cell fabricated with mixed NH_2-UiO-66(Zr/Ti) shows higher photon-to-current efficiency than NH_2-UiO-66(Zr). This study illustrates the potential of TAS as a tool to provide spectroscopic data of the photophysics of MOFs whose better understanding can lead to a rational design of MOFs as photo-responsive materials.

ASSOCIATED CONTENT

Supporting Information. A detailed list with all the chemical reagents employed. Characterization techniques. ATR-FTIR spectra, nitrogen isotherms, thermogravimetric analysis and SEM images of the prepared MOFs. TAS data mentioned on the manuscript.

AUTHOR INFORMATION

The authors declare no competing financial interests.

ACKNOWLEDGMENTS

Financial support by the Spanish Ministry of Economy and Competitiveness (CTQ2014-53292-R-AR, Severo Ochoa, CTQ2015-69153-CO_2-R) is gratefully acknowledged. S.N. thanks financial support by Fundación Ramón Areces (XVIII Concurso Nacional, Ciencias de la Vida y de la Materia, Energía renovable: materiales y procesos 2016).

REFERENCES

(1) Kubacka, A.; Fernández-García M.; Colón, G. Advanced nanoarchitectures for solar photocatalytic applications. *Chem. Rev.* **2012**, *112*, 1555-1614.

(2) Chen, H.; Nanayakkara, C. E.; Grassian, V. H. Titanium dioxide photocatalysis in atmospheric chemistry. *Chem. Rev.* **2012**, *112*, 5919-5948.

(3) Esswein A. J.; Nocera, D. G. Hydrogen production by molecular photocatalysis. *Chem. Rev.* **2007**, *107*, 4022-4047.

(4) Inoue, T.; Fujishima, A.; Konishi, S.; Honda, K. Photoelectrocatalytic reduction of carbon dioxide in aqueous suspensions of semiconductor powders. *Nature* **1979**, *277*, 637-638.

(5) Matsuoka, M.; Anpo, M. J. Local structures, excited states, and photocatalytic reactivities of highly dispersed catalysts constructed within zeolites. *Photochem. Photobiol., C* **2003**, *3*, 225-252.

(6) Indrakanti, V. P.; Kubicki, J. D.; Schobert, H. H. Photoinduced activation of CO_2 on Ti-based heterogeneous catalysts: current state, chemical physics-based insights and outlook. *Energy Environ. Sci.* **2009**, *2*, 745-758.

(7) Wang, W.; Wang, S.; Ma, X.; Gong, J. Recent advances in catalytic hydrogenation of carbon dioxide. *Chem. Soc. Rev.* **2011**, *40*, 3703-3727.

(8) Chen, X.; Shen, S.; Guo, L.; Mao, S. S. Semiconductor-based photocatalytic hydrogen generation. *Chem. Rev.* **2010**, *110*, 6503-6570.

(9) Lang, X.; Chen X.; Zhao, J. Heterogeneous visible light photocatalysis for selective organic transformations. *Chem. Soc. Rev.* **2014**, *43*, 473-486.

(10) Tong, H.; Ouyang, S. X.; Bi, Y. P.; Umezawa, N.; Oshikiri, M.; Ye, J. H. Nano-photocatalytic materials: possibilities and challenges. *Adv. Mater.* **2012**, *24*, 229-251.

(11) Dhakshinamoorthy, A.; Asiri, A. M.; Garcia, H. Metal-organic framework (MOF) compounds: photocatalysts for redox reactions and solar fuel production. *Angew. Chem., Int. Ed.* **2016**, *55*, 5414-5445.

(12) Wang, C.; Liu, D.; Lin, W. Metal–organic frameworks as a tunable platform for designing functional molecular materials. *J. Am. Chem. Soc.* **2013**, *135*, 13222-13234.

(13) Zhang, T.; Lin, W. Metal–organic frameworks for artificial photosynthesis and photocatalysis. *Chem. Soc. Rev.* **2014**, *43*, 5982-5993.

(14) Fu, Y.; Sun, D.; Chen, Y.; Huang, R.; Ding, Z.; Fu, X.; Li, Z. An amine-functionalized titanium metal-organic framework photocatalyst with visible-light-induced activity for CO_2 reduction. *Angew. Chem., Int. Ed.* **2012**, *51*, 3364-3367.

(15) Zhang, H.; Liu, G.; Shi, L.; Liu, H.; Wang, T.; Ye, J. Engineering coordination polymers for photocatalysis. *Nano Energy* **2016**, 22, 149-168.

(16) Wang, S.; Wang, X. Multifunctional metal-organic frameworks for photocatalysis. *Small* **2015**, *11*, 3097-3112.

(17) Nasalevich, M. A.; van der Veen, M.; Kapteijn, F.; Gascon, J. Metal–organic frameworks as heterogeneous photocatalysts: advantages and challenges. *CrystEngComm* **2014**, *16*, 4919-4926.

(18) Horiuchi, Y.; Toyao, T.; Takeuchi, M.; Matsuoka, M.; Anpo, M. Recent advances in visible-light-responsive photocatalysts for hydrogen production and solar energy conversion-from semiconducting TiO_2 to MOF/PCP photocatalysts. *Phys. Chem. Chem. Phys.* **2013**, *15*, 13243-13253.

(19) Alvaro, M.; Carbonell, E.; Ferrer, B.; Llabrés i Xamena, F. X.; Garcia, H. Semiconductor behavior of a metal-organic framework (MOF). *Chem. Eur. J.* **2007**, *13*, 5106-5112.

(20) Tachikawa, T.; Choi, J. R.; Fujitsuka, M.; Majima, T. Photoinduced charge-transfer processes on MOF-5 nanoparticles: elucidating differences between metal-organic frameworks and semiconductor metal oxides. *J. Phys. Chem. C* **2008,** *112*, 14090-14101.

(21) Gomes Silva, C. G.; Luz, I.; LlabrésiXamena, F. X.; Corma, A.; Garcia, H. Water stable Zr-benzenedicarboxylate metal-organic frameworks as photocatalysts for hydrogen generation. *Chem. Eur. J.* **2010**, *16*, 11133-11138.

(22) Horiuchi, Y.; Toyao, T.; Saito, M.; Mochizuki, K.; Iwata, M.; Higashimura, H.; Anpo, M.; Matsuoka, M. J. Visible-light-promoted photocatalytic hydrogen production by using an amino-functionalized Ti(IV) metal–organic framework. *J. Phys. Chem. C* **2012**, *116*, 20848-20853.

(23) Nasalevich, M. A.; Becker, R.; Ramos-Fernandez, E. V.; Castellanos, S.; Veber, S. L.; Fedin, M. V.; Kapteijn, F.; Reek, J. N. H.; van der Vlugt, J. I.; Gascon, J. Co@NH_2-MIL-125(Ti): cobaloxime-derived metal–organic framework-based composite for light-driven H_2 production . *Energy Environ. Sci.* **2015**, *8*, 364-375.

(24) Li, Z.; Xiao, J.-D.; Jiang, H.-L. Encapsulating a Co(II) molecular photocatalyst in metal-organic framework for visible-light driven H_2 production: boosting catalytic efficiency via spatial charge separation. *ACS Catal.* **2016**, *6*, 5359-5365.

(25) Wang, D. K.; Huang, R. K.; Liu, W. J.; Sun, D. R.; Li, Z. H. Fe-based MOFs for photocatalytic CO_2 reduction: role of coordination unsaturated sites and dual excitation pathways. *ACS Catal.* **2014**, *4*, 4254-4260.

(26) Sun, D. R.; Fu, Y. H.; Liu, W. J.; Ye, L.; Wang, D. K.; Yang, L.; Fu, X. Z.; Li, Z. H. Studies on photocatalytic CO_2 reduction over NH_2-Uio-66(Zr) and its derivatives: towards a better understanding of photocatalysis on metal–organic frameworks. *Chem. - Eur. J.* **2013**, *19*, 14279-14285.

(27) Xu, H.; Hu, J.; Wang, D.; Li, Z.; Zhang, Q.; Luo, Y.; Yu, S.; Jiang, H. Visible-light photoreduction of CO_2 in a metal−organic framework: boosting electron−hole separation via electron trap states. *J. Am. Chem. Soc.* **2015**, *137*, 13440-13443.

(28) Wang, M.; Wang, D.; Li, Z. Self-assembly of CPO-27-Mg/TiO_2 nanocomposite with enhanced performance for photocatalytic CO_2 reduction. *Appl. Catal. B: Environ.* **2016**, 183, 47-52.

(29) Wang, D. K.; Li, Z. H. Bi-functional NH_2-MIL-101IJFe) for one-pot tandem photo-oxidation/Knoevenagel condensation between aromatic alcohols and active methylene compounds. *Catal. Sci. Technol.* **2015**, *5*, 1623-1628.

(30) Sun, D. R.; Ye, L.; Li, Z. H. Visible-light-assisted aerobic photocatalytic oxidation of amines to imines over NH_2-MIL-125(Ti) *Appl. Catal. B* **2015**, *164*, 428-432.

(31) Manna, K.; Zhang, T.; Greene, F. X.; Lin, W. B. Bipyridine- and phenanthroline-based metal-organic frameworks for highly efficient and tandem catalytic organic transformations via directed C-H activation. *J. Am. Chem. Soc.* **2015**, *137*, 2665-2673.

(32) D. Wang, M. Wang, Z. Li, Fe-Based Metal–Organic Frameworks for Highly Selective Photocatalytic Benzene Hydroxylation to Phenol. *ACS Catal.* **2015**, *5*, 6852-6857.

(33) Wang, D.; Li, Z. Coupling MOF-based photocatalysis with Pd catalysis over Pd@MIL-100(Fe) for efficient N-alkylation of amines with alcohols under visible light *J. Catal.* **2016**, *342*, 151-157.

(34) Sun, D.; Li, Z.; Double-Solvent Method to Pd Nanoclusters Encapsulated inside the Cavity of NH_2–Uio-66(Zr) for Efficient Visible-Light-Promoted Suzuki Coupling Reaction *J. Phys. Chem. C* **2016**, *120*, 19744-19750.

(35) Fateeva, A.; Chater, P. A.; Ireland, C. P.; Tahir, A. A.; Khimyak, Y. Z.; Wiper, P. V.; Darwent, J. R.; Rosseinsky, M. J. A water-stable porphyrin-based metal–organic framework active for visible-light photocatalysis. *Angew. Chem. Int. Ed.* **2012**, *51*, 7440-7444.

(36) Laurier, K. G. M.; Vermoortele, F.; Ameloot, R.; De Vos, D. E.; Hofkens, J.; Roeffaers, M. B. J. Synthesis modulation as a tool to increase the catalytic activity of metal-organic frameworks: the unique case of UiO-66(Zr). *J. Am. Chem. Soc.* **2013**, *135*, 11465-11468.

(37) Wang, C.; Li, J.; X.Lv, Zhang, Y.; Guo, G. Photocatalytic organic pollutants degradation in metal–organic frameworks. *Energy Environ. Sci.* **2014**, *7*, 2831-2867.

(38) Dias, Elton M.; Petit, Camille. Towards the use of metal–organic frameworks for water reuse: a review of the recent advances in the field of organic pollutants removal and degradation and the next steps in the field. *J. Mater. Chem. A* **2015**, *3*, 22484-22506

(39) Navarro Amador R.; Carboni, M.; Meyer, D. Photosensitive titanium and zirconium Metal Organic Frameworks: current research and future possibilities. *Materials Letters* **2016**, *166*, 327-338.

(40) Hendon, C. H.; Tiana, D.; Fontecave, M.; Sanchez, C.; D'arras, L.; Sassoye, C.; Rozes, L.; Mellot‐Draznieks, C.; Walsh, A. Engineering the optical response of the titanium-MIL-125 metal-organic framework through ligand functionalization. *J. Am. Chem. Soc.* **2013**, *135*, 10942-10945.

(41) Musho, T.; Li, J.; Wu, N. Band gap modulation of functionalized metal-organic frameworks. *Phys. Chem. Chem. Phys.***2014**, *16*, 23646-23653.

(42) Flage-Larsen, E.;Røyset, A.;Cavka, J. H.;Thorshaug, K. Band gap modulations in UiO metal–organic frameworks. *J. Phys. Chem. C* **2013**, *117*, 20610-20616.

(43) Hendrickx, K.;Vanpoucke, D. E. P.;Leus, K.;Lejaeghere, K.;Yperen-De Deyne, A. V.;Speybroeck, V. V.; Van Der Voort, P.;Hemelsoet, K. Understanding intrinsic light absorption properties of UiO-66 frameworks: a combined theoretical and experimental study. *Inorg. Chem.* **2015**, *54*, 10701-10710.

(44) Yasin, A. S.; Li, J.; Wu, N.; Musho, T. Study of the inorganic substitution in a functionalized UiO-66 metal–organic framework. *Phys. Chem. Chem. Phys.* **2016**, *18*, 12748-12754.

(45) Cavka, J. H.; Jakobsen, S.; Olsbye, U.; Guillou, N.; Lamberti, C.; Bordiga, S.; Lillerud, K. P. A new zirconium inorganic building brick forming metal organic frameworks with exceptional stability. *J. Am. Chem. Soc.* **2008**, *130*, 13850-13851.

(46) Shen, L. J.; Liang, R. W.; Luo, M. B.; Jing, F. F.; Wu, L. Electronic effects of ligand substitution on metal-organic framework photocatalysts: the case study of UiO-66**.** *Phys. Chem. Chem. Phys.* **2015**, *17*, 117-121.

(47) Long, J.; Wang, S.; Ding, Z.; Wang, S.; Zhou, Y.; Huang, L.; Wang, X. Amine-functionalized zirconium metal-organic framework as efficient visible-light photocatalyst for aerobic organic transformations. *Chem. Commun.* **2012**, *48*, 11656-11658.

(48) Nasalevich, M. A.; Hendon, C. H.; Santaclara, J. G.; Svane, K.; van der Linden, B.; Veber, S. L.; Fedin, M. V.; Houtepen, A. J.; van der Veen, M. A.; Kapteijn, F.; Walsh, A.; Gascon, J. Electronic origins of photocatalytic activity in d(0) metal organic frameworks. *Sci. Rep.* **2016**, *6*, 23676, 1-9.

(49) Sun, D.; Liu, W.; Qiu, M.; Zhang, Y.; Li, Z. Introduction of a mediator for enhancing photocatalytic performance via post-synthetic metal exchange in metal–organic frameworks (MOFs). *Chem. Commun.* **2015**, *51*, 2056-2059.

(50) Lee, Y.; Kim, S.; Kang, J. K.; Cohen, S. M. Photocatalytic CO_2 reduction by a mixed metal (Zr/Ti), mixed ligand metal–organic framework under visible light irradiation. *Chem. Commun.* **2015**, *51*, 5735-5738.

(51) Li, Y.-F.; Xu, D.; Oh, J. I.; Shen, W.; Li, X.; Yu, Y. Mechanistic study of codoped titania with nonmetal and metal ions: A case of C + Mo codoped TiO_2. *ACS Catal.* **2012**, *2*, 391-398.

(52) Kameneva, O.; Kuznestov, A. I.; Smirnova, L. A.; Rozes, L.; Sanchez, C.A. Alexandrov; Bityurin, N.; Chhor, K.; Kanaev, *J. Mater. Chem.* **2005**, *15*, 3380-3383.

(53) Kuznetsov, A. I.; Kameneva, O.; Bityurin, N.; Rozes, L.; Sanchez, C.; Kanaev, A. Laser-induced photopatterning of organic–inorganic TiO_2-based hybrid materials with tunable interfacial electron transfer. *Phys. Chem. Chem. Phys.* **2009**, *11*, 1248–1257.

(54) Dan-Hardi, M.; Serre, C.; Frot, T.; Rozes, L.; Maurin, G.; Sanchez, C.; Ferey, G. A new photoactive crystalline highly porous titanium(IV) dicarboxylate *J. Am. Chem. Soc.* **2009**, *131*, 10857–10859.

(55) De Miguel, M.; Ragon, F.; Devic, T.; Serre, C.; Horcajada, P.; Garcia, H. Evidence of photoinduced charge separation in the metal-organic framework MIL-125(Ti)-NH_2. *ChemPhysChem* **2012**, *13*, 3651–3654.

(56) Walsh, A.; Catlow, C. R. A. Photostimulated reduction processes in a titania hybrid metal–organic framework. *ChemPhysChem* **2010**, *11*, 2341–2344.

(57) Santaclara, J. G.; Nasalevich, M. A.; Castellanos, S.; Evers, W. H.; Spoor, F. C. M.; Rock, K.; Siebbeles, L. D. A.; Kapteijn, F.; Grozema, F.; Houtepen, A.; Gascon, J.; Hunger, J.; van der Veen, M. A. Organic linker defines the excited-state decay of photocatalytic MIL-125(Ti)-type Materials. *ChemSusChem* **2016**, *9*, 388 – 395.

(58) Lopez, H. A.; Dhakshinamoorthy, A.; Ferrer, B.; Atienzar, P.; Alvaro, M.; Garcia, H. Photochemical response of commercial MOFs: $Al_2(BDC)_3$ and its use as active material in photovoltaic devices. *J. Phys. Chem. C* **2011**, *115*, 22200–22206.

(59) Xie, T.-H.; Sun, X. ; Lin, J. Enhanced photocatalytic degradation of RhB driven by visible light-induced MMCT of Ti(IV)−O−Fe(II) formed in Fe-doped $SrTiO_3$. *J. Phys. Chem. C* **2008**, *112*, 9753–9759.

(60) Nakamura, R.; Okamoto, A.; Osawa, H.; Irie, H.; Hashimoto K. Design of all-inorganic molecular-based photocatalysts sensitive to visible light: Ti(IV)−O−Ce(III) bimetallic assemblies on mesoporous silica. *J. Am. Chem. Soc.* **2007**, *129*, 9596-9597.

(61) Turlington, M. D.; Pienkos, J. A.; Carlton, E. S.; Wroblewski, K. N.; Myers, A. R.; Trindle, C. O.; Altun, Z.; Rack, J. J.; Wagenknecht, P. S. Complexes with tunable intramolecular ferrocene to Ti^{IV} electronic transitions: models for solid state Fe^{II} to Ti^{IV} charge transfer. *Inorg. Chem.* **2016**, *55*, 2200−2211.

TOC GRAPHICS